2009-9

Performance Flight Testing of Small Electric Powered Unmanned Aerial Vehicles

Jon N. Ostler
Brigham Young University - Provo

W. Jerry Bowman
Brigham Young University - Provo, jbowman@et.byu.edu

See next page for additional authors

Original Publication Citation
Jon N. Ostler, W. Jerry Bowman, Deryl O. Snyder, and Timothy W. McLain. "Performance Flight Testing of Small, Electric Powered Unmanned Aerial Vehicles". International Journal of Micro Air Vehicles, Volume 1, Number 3, 2009.

Authors
Jon N. Ostler, W. Jerry Bowman, Deryl O. Snyder, and Timothy W. McLain

Performance Flight Testing of Small, Electric Powered Unmanned Aerial Vehicles

Jon N. Ostler*, W. Jerry Bowman†, Deryl O. Snyder‡ and Timothy W. McLain§
Brigham Young University, Provo Utah, 84602, USA

ABSTRACT

Flight testing methods are developed to find the drag polar for small unmanned aerial vehicles powered by electric motors with fixed-pitch propellers. Wind tunnel testing was used to characterize the propeller-motor efficiency. The drag polar was constructed using data from flight tests. This drag polar was then used to find the following performance parameters: maximum velocity, minimum velocity, velocity for maximum range, velocity for maximum endurance, maximum rate of climb, maximum climb angle, minimum turn radius, maximum turn rate, and maximum bank angle. The developed flight testing methods are used to characterize the performance of a small UAV.

NOMENCLATURE

C	battery energy capacity (joules)
C_D	coefficient of drag
C_{D_o}	zero lift drag coefficient
C_L	coefficient of lift
D	drag
E	voltage
i	current
K	induced drag constant
K_1	constant
K_2	constant
L	lift
n	load factor
P_a	power available
P_e	electrical power
P_{out}	power out
P_r	power required
R	turn radius
R/C	rate of climb
S	wing area
T	thrust
T_r	thrust required
V	airspeed
W	weight
γ	climb angle
η	motor-propeller efficiency
ρ	fluid density
ω	turn rate
ϕ	bank angle

*Masters Student, Mechanical Engineering, AIAA Student Member

†Associate Professor, Mechanical Engineering, AIAA Senior Member

‡Assistant Professor, Mechanical Engineering, AIAA Member

§Professor and Chair, Mechanical Engineering, AIAA Associate Fellow

I. INTRODUCTION

Small, electric powered, unmanned aerial vehicles (UAVs) are a subclass of UAVs that do not lend themselves directly to flight testing methods developed for larger aircraft that are powered by gas turbine or reciprocating engines. Examples of small electric planes are Lockheed Martin's Desert Hawk and AeroVironment's DragonEye. Traditional flight testing methods are not acceptable for small UAVs for the following reasons. First, in-flight engine power cannot be determined by measuring fuel flow, as it is done for engines that burn fuel. Second, electric powered UAVs do not decrease in weight over time as fuel burning planes do. Finally data acquisition systems in small UAVs are limited in size and weight.

Flight test methods for large manned airplanes powered by gas turbine and reciprocating engines have been well established for many years. An abundance of literature exists that describes flight test methods for large aircraft. Recent research has begun to build the body of knowledge for many aspects of flight testing small UAVs. There is available literature that discusses flight testing small UAVs to quantify stability and dynamics[1,2]. Flight testing has also been done to observe the usefulness of the latest developments, such as a new control law[3] or a novel wing structure[4]. Some writing has been published that discusses flight testing scale models for the purpose of discerning characteristics of full-size aircraft[5,6]. However, there appears to be a shortage of published material that addresses performance flight testing for small electric UAVs.

Williams and Harris[7] briefly address the perceived difficulties in performance flight testing of small UAVs. Hiller[8] finds a drag polar using descent methods,but does so to determine the effect of flaps on drag and does not discuss performance. Abdulrahim[9] finds the glide slope and rate of climb for a biologically inspired UAV, but does not look at other performance parameters or find the drag polar.

This work develops flight test methods for small unmanned aerial vehicles powered by electric motors with fixed pitch-propellers. A reliable technique for finding the drag polar is presented. In addition, the equations and graphical methods needed to calculate maximum velocity, minimum velocity, velocity for maximum range, velocity for maximum endurance, maximum rate of climb, maximum climb angle, and turn performance are developed.

II. APPROACH

When quantifying the performance of an aircraft, the most important information that can be derived from flight tests is the drag polar. Kimberlin says it this way, "If the drag polar of an aircraft is accurately determined and the thrust, or thrust horsepower, available is known, then all of the performance characteristics of the subject airplane may be calculated."[10] The approach taken here is to first determine the drag polar from flight tests and then calculate other performance parameters from this drag polar. When possible, the parameters found from calculations are validated with further flight tests.

III. FINDING THE DRAG POLAR FROM FLIGHT TESTS

A. Theory

The drag polar is useful in characterizing an aircraft because it is dependent on distinguishing features including the weight of the aircraft, the airfoil used, protuberances, and the shape of the fuselage. Also, important is the fact that the drag polar can be used to calculate other performance parameters. One form of the drag polar is described by the equation

$$C_D = C_{D_o} + K_2 C_L + K_1 C_L^2 \tag{1}$$

If the assumption is made that minimum drag occurs at zero lift, the drag polar can be expressed as

$$C_D = C_{D_o} + K C_L^2. \tag{2}$$

While this assumption is valid for many aircraft, steps should be taken to verify its usability for the aircraft being flight tested.

In order to measure the drag polar for a small UAV, C_D and C_L must be reduced to measurable parameters. Once C_D and C_L have been found for various flight conditions, graphical methods can be used to find the remaining constants present in Eq. (1) or (2). Assuming steady level flight, the equations of flight are

$$W = L = \frac{1}{2}\rho V^2 C_L S \tag{3}$$

and

$$T_r = D = \frac{1}{2}\rho V^2 C_D S. \tag{4}$$

The power required for steady level flight can be found by multiplying both sides of Eq. (4) by velocity, which then becomes

$$P_r = T_r V = \frac{1}{2}\rho V^3 C_D S. \tag{5}$$

If the efficiency of the propeller-electric motor combination is known, then the relationship between the mechanical power required for flight (P_r) and the electrical power (P_e) supplied to the motor is described by

$$P_r = \eta P_e. \tag{6}$$

Electrical power can also be formed from the product of the voltage and the current into the electric motor

$$P_e = iE. \tag{7}$$

Combining Eq. (5), (6), and (7) and solving for C_D gives

$$C_D = \frac{2iE\eta}{\rho V^3 S}. \tag{8}$$

Eq. (3) can be solved for C_L to give

$$C_L = \frac{2W}{\rho V^2 S}. \tag{9}$$

All of the variables on the right hand sides of Eq. (8) and (9) can be measured for a given airplane in a given flight condition. The only remaining parameters in the drag polar that are not known are C_{D_o} and either K_2 and K_1, or $K.C_{D_o}$, K_2, and K_1 can be found graphically by plotting C_D verses C_L and then fitting the data with a second order polynomial in order to find the constants. In the case of the simplified drag polar, if C_D is plotted verses C_L^2 as shown in Fig. 1, the slope of this plot is equal to K and the y-intercept is equal to C_{D_o}.

B. Ground Test Methods

Before the drag polar can be found from flight tests, the efficiency of the motor-propeller combination must be determined over the range of possible throttle settings and vehicle velocities. The motor-propeller efficiency can be found from wind tunnel tests,where an electric motor and propeller are mounted on a force balance and the thrust produced is measured for various air speeds. The thrust multiplied by the velocity of the air moving through the wind tunnel is the mechanical power out. The ratio of the mechanical power to the electrical power supplied to the motor is the efficiency:

$$\eta = \frac{P_{out}}{P_e} = \frac{TV}{iE}. \tag{10}$$

Once the motor-propeller efficiency is measured over a range of power settings and wind tunnel air speeds, a two dimensional look-up table can then be created with P_e, V, as the inputs and η as the output. This look-up table is used to determine the operating efficiency of the motor-propeller combination.

During wind tunnel testing the maximum thrust is also recorded for each airspeed. These values are used to construct the thrust available and power available curves, which can then be used in the calculation of other performance parameters. Other vital data to gather prior to flight testing are the

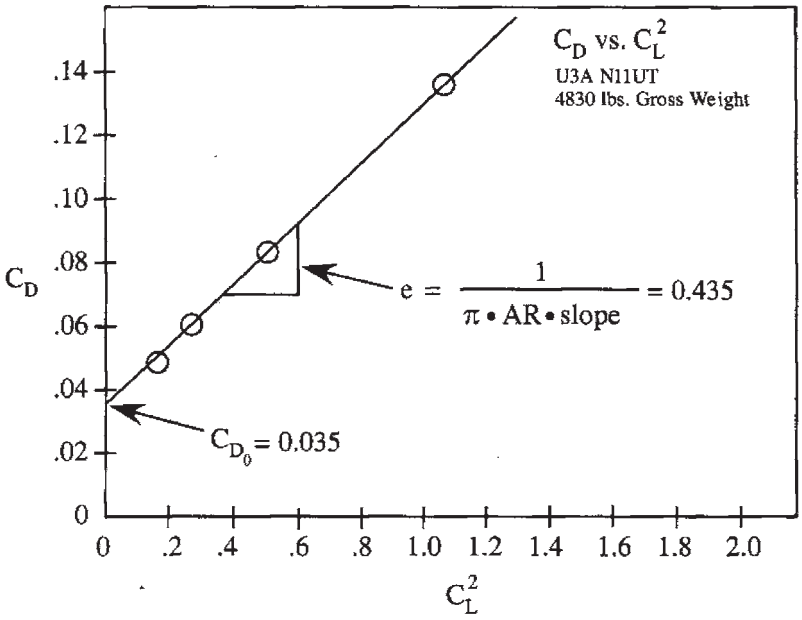

Figure 1. Example plot of C_D vs C_L^2 (from Kimberlin[10]).

aircraft's total weight, wing area, the air temperature, and the barometric pressure. Air temperature and barometric pressure are used to calculate air density.

C. Flight Test Method

After ground testing has been performed, the only parameters still needed to calculate C_L and C_D from Eq. (8) and (9) are airspeed, current, and voltage. If these parameters are measured while the test aircraft is at a constant velocity on a straight level course, then C_L can be plotted verses C_D, thus creating one point of the drag polar. When this process is repeated for multiple velocities, an approximation of the drag polar can be determined. Therefore, an appropriate flight test is to fly the UAV in a straight and level path at a constant throttle setting over a large distance. During each constant-throttle run airspeed, current, and voltage are measured and recorded multiple times. These data points are then averaged and used to estimate precision error. Multiple runs, at a range of throttle settings, are performed to create the C_L verses C_D curve.

D. Alternative Methods

The method just described has been successfully used to find the drag polar of a small electric powered UAV and the results will be presented later. Two alternative methods could also be used. First if the position of a small UAV can be accurately estimated, then the glide polar method described by Kimberlin may be used[10]. A third method is similar to what has been presented but involves measuring the RPM of the propeller in flight. RPM sensors are available that are small enough to be mounted on a small UAV. If one of these sensors were integrated into the data acquisition system on the test aircraft then the following method could be used.

Starting with Eq. (3) and Eq. (4) given above and solving for C_L and C_D respectively, yields

$$C_L = \frac{2W}{\rho V^2 S} \tag{11}$$

$$C_D = \frac{2T_r}{\rho V^2 S}. \tag{12}$$

The T_r term in Eq. (12) could be found from wind tunnel testing in a similar manner to that described for efficiency. The thrust produced by the motor-propeller combination and the RPM of the propeller would be measured at various throttle and airspeed settings in a wind tunnel. This would make

it possible to create a two dimensional thrust look-up table. The thrust look-up table would be used to determine the thrust produced by the propeller for specific RPM and airspeed measurements taken during flight tests.This method does require adding more hardware to the data acquisition system. However, it has the potential to be more accurate, because it does not depend on a knowledge of motor efficiency which could change with use and shifting environmental conditions.

IV. FINDING PERFORMANCE PARAMETERS FROM THE DRAG POLAR

After the drag polar has been found for a particular aircraft it can be used to calculate important performance parameters including power required, rate of climb, range, endurance, minimum turn radius, maximum turn rate, minimum bank angle, and maximum velocity.The methods presented in this section are based the expanded drag polar of Eq. (1).

A. Power Required

The drag polar can be used to construct the power required curve. Solving Eq. (3) and Eq. (4) for C_L and C_D gives

$$C_L = \frac{2W}{\rho V^2 S} \tag{13}$$

$$C_D = \frac{2P_r}{\rho V^3 S}. \tag{14}$$

Substituting Eq. (13) and Eq. (14) into the drag polar equation and solving for power required gives

$$P_r = C_{D_o} \frac{1}{2}\rho V^3 S + K_2 W V + \frac{K_1 W^2}{\frac{1}{2}\rho V S}. \tag{15}$$

The only term in Eq. (15) that is not constant is velocity. Power required can be plotted as a function of velocity as shown in Fig. 2. Note that an expression for thrust required can be found by dividing both sides of Eq. (15) by velocity.

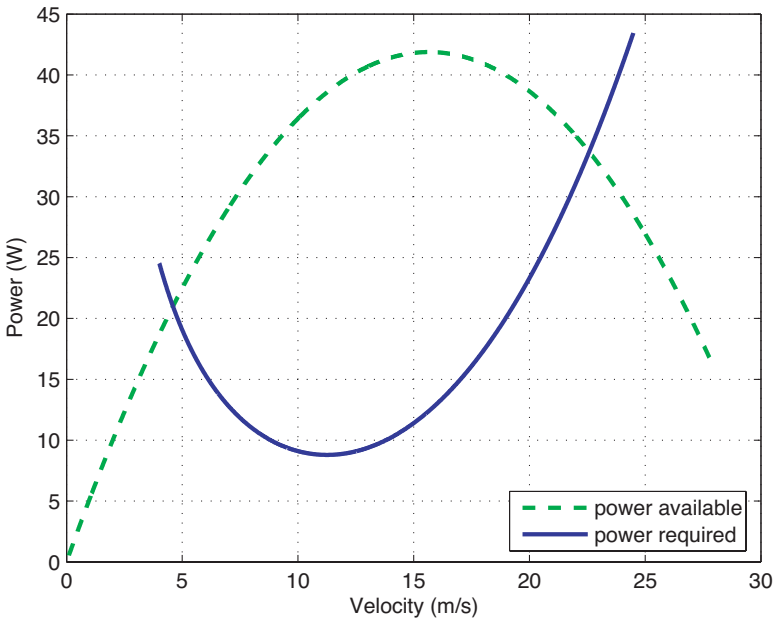

Figure 2. Example power required curve.

B. Maximum Velocity and Rate of Climb

Fig. 2 displays the power required curve and the power available curve (found from wind tunnel testing) and can be used to find maximum velocity. On the right side of the plot, the velocity at which the power available curve crosses the power required curve indicates maximum velocity.

The difference between the power available curve and the power required curve represents the excess power or the power available for constant velocity climbing flight. Rate of climb is equal to excess power divided by the weight of the airplane[11] and is given by Eq. (16). A plot of rate of climb verses velocity can be seen in Fig. 3.

$$R/C = \frac{P_a - P_r}{W} \tag{16}$$

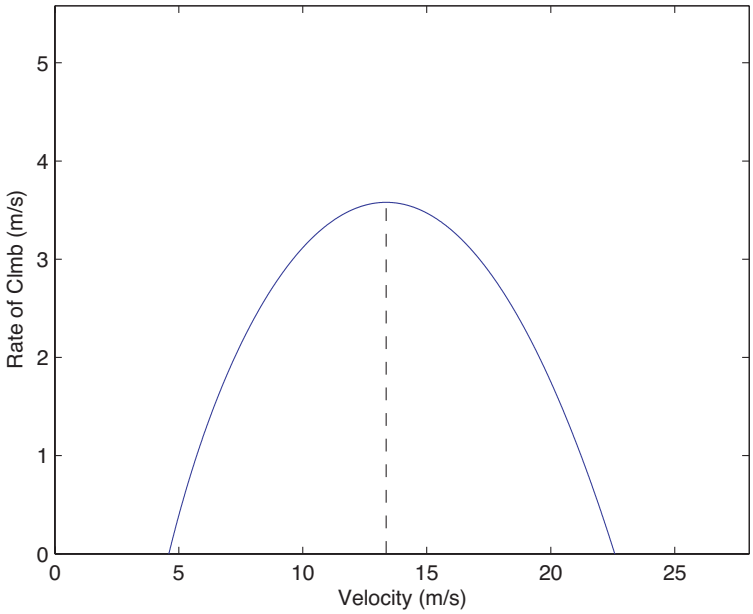

Figure 3. Example rate of climb plot.

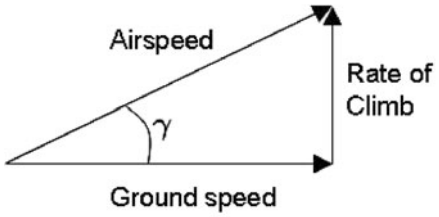

Figure 4. Climbing velocities.

The diagram in Fig. 4 illustrates the relationship between airspeed, ground speed, and rate of climb for unaccelerated climbing. The climb angle γ is given by

$$\gamma = \arcsin\left(\frac{R/C}{V}\right), \tag{17}$$

where V is the airspeed of the aircraft. Eq. (17) can be used together with the rate of climb plot to create a plot of climb angle verses velocity. The maximum climb angle can then be determined from this plot.

C. Range and Endurance

The power required curve can further be used to find the velocity at which an airplane should fly in order to achieve maximum endurance. Endurance is maximized when power required is minimized.

This is shown graphically in Fig. 5(a). Similarly, maximum range is achieved when the thrust required is a minimum. An example plot of thrust required is shown in Fig. 5(b).

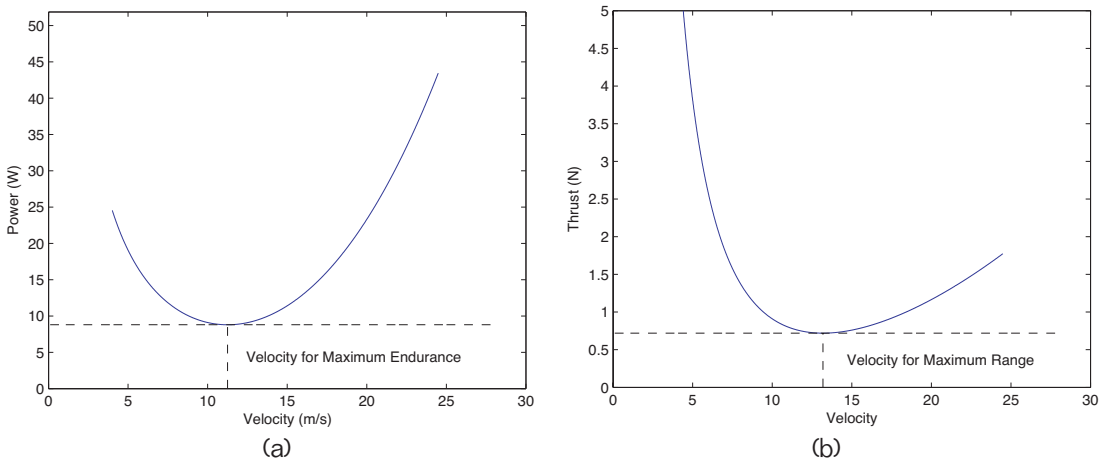

Figure 5. Velocity for maximum range and maximum endurance.

D. Turn Performance

Minimum turn radius, maximum turn rate, and maximum bank angle for a UAV in a steady, level turn can be found using the drag polar generated from flight testing. Many of the following thoughts and derivations are patterned after Anderson[12], the main difference being that the form of the drag polar used here makes no assumption that minimum drag occurs at zero lift.

Anderson provides the following equations for turn radius R, turn rate ω, and bank angle ϕ assuming a constant-velocity level turn

$$R = \frac{V^2}{g\sqrt{n^2 - 1}} \tag{18}$$

$$\omega = \frac{g\sqrt{n^2 - 1}}{V^2} \tag{19}$$

$$\phi = \arccos\frac{1}{n}. \tag{20}$$

The load factor n is defined as L/W. In order to minimize turn radius, velocity needs to be minimized and the load factor maximized. Maximizing turn rate also requires that velocity be minimized and the load factor maximized. It is important to note however, that the load factor is constrained by both the maximum coefficient of lift, or stall, and the thrust available.

The equations of flight for a steady level turn, can be used to derive a relationship between the load factor and thrust available:

$$L = nW = \frac{1}{2}\rho V^2 C_L S \tag{21}$$

$$T = D = \frac{1}{2}\rho V^2 C_D S. \tag{22}$$

Solving for C_L and C_D gives

$$C_L = \frac{2nW}{\rho V^2 S} \tag{23}$$

and

$$C_D = \frac{2T}{\rho V^2 S}. \tag{24}$$

Substituting C_L and C_D into the drag polar (Eq. (1)) yields the following equation.

$$\frac{2T}{\rho V^2 S} = C_{D_o} + K_2\left(\frac{2nW}{\rho V^2 S}\right) + K_1\left(\frac{2nW}{\rho V^2 S}\right)^2 \tag{25}$$

Finally, solving for n and keeping only the positive solution gives

$$n = \frac{-K_2 W + \sqrt{(K_2 W)^2 - 4K_1 W^2\left(C_{D_o} + \frac{2T}{\rho V^2 S}\right)}}{\frac{4K_1 W^2}{\rho V^2 S}}. \tag{26}$$

Using the thrust available data, the maximum load factor can be plotted with respect to velocity as shown in Fig. 6. This plot provides a visual representation of how the load factor is limited by the thrust available.

The definition of the load factor can be used to derive its limiting value in terms of the maximum coefficient of lift

$$n \equiv \frac{L}{W} = \frac{\rho V^2 C_L S}{2W}. \tag{27}$$

In the limiting condition C_L becomes $(C_L)_{max}$

$$n_{max} = \frac{\rho V^2 (C_L)_{max} S}{2W}. \tag{28}$$

A plot of load factor verses velocity for both the thrust available condition and the maximum lift coefficient condition is shown in Fig. 6. It should be noted that the load factor is also constrained by the structural limits of the aircraft,[12] which are not discussed here.

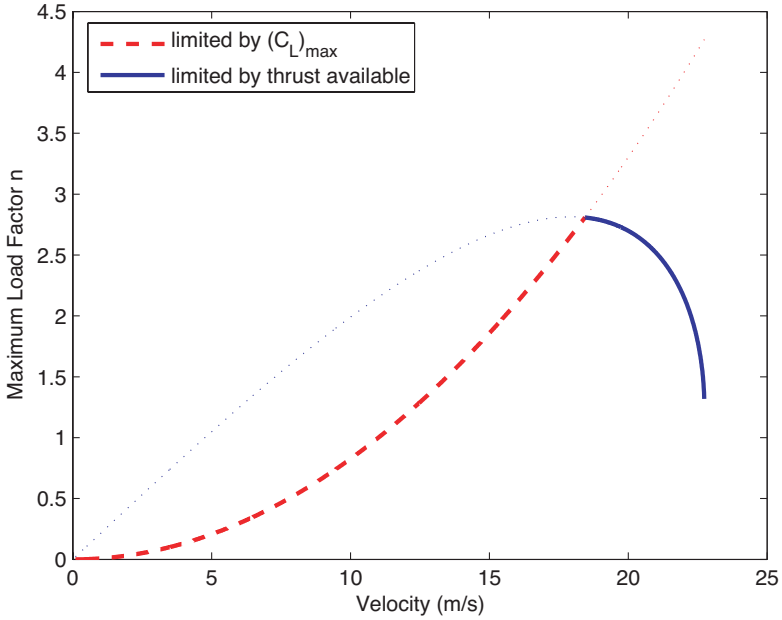

Figure 6. Maximum load factor verses velocity for the two limiting conditions.

Fig. 6 provides the necessary information needed to calculate turn radius, turn rate, and bank angle for a given velocity. These parameters can be plotted with respect to velocity. Maximum and minimum values can be determined graphically. Example plots of minimum turn radius and maximum turn rate are shown below in Fig. 7. These plots were found by combining the results of Fig. 6 with Eq. (18) for turn radius and Eq. (19) for turn rate. Notice that both limiting conditions are represented.

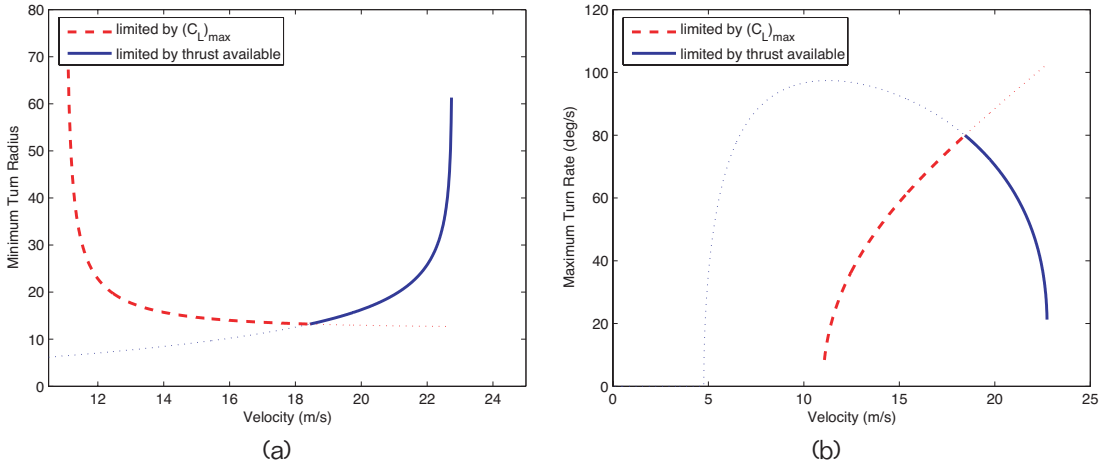

Figure 7. (a) Minimum turn radius. (b) Maximum turn rate.

For the minimum turn radius plot, all feasible turn radii are represented by the area above the bolded curves. At a given velocity the bolded curves represent the minimum turn radius for that velocity. For the maximum turn rate plot, the feasible flight regime lies below the bolded curves.

V. RESULTS

This section discusses the actual flight testing of a small electric UAV. The first two subsections give a brief description of the test aircraft, data acquisition system, and related hardware. The remaining subsections present the results of ground testing, the drag polar, and the performance of the aircraft.

A. Hardware

The test aircraft chosen for this work was a commercially available flying wing called Unicorn. The Unicorn is made of expanded polypropylene (EPP) foam, supported with carbon spars and covered with Monokote. This plane was chosen for testing because it is inexpensive and durable. The Unicorn that

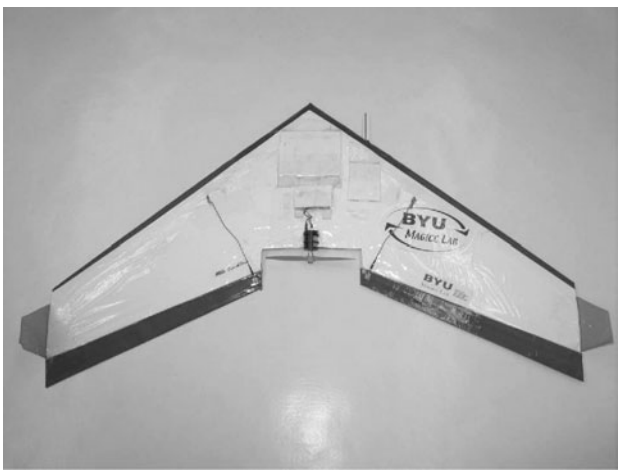

Figure 8. Unicorn small UAV used in flight tests.

was flight tested is shown in Fig. 8. The wing span measured 1.06 m. The wing area S was 0.321 m^2 and the complete airplane weight, including batteries, was 9.34 N, (approximately 2 lb).

The propulsion system for the test aircraft was a MEGA 16/15/6 brushless electric motor with a 7 × 4 inch propeller. Electric power was provided by two Kokam 11.1 V, 1500 mAh lithiumpolymer batteries in parallel.

B. Data Acquisition

Data acquisition and control of the test aircraft was achieved using the Kestrel 2.0 autopilot and a ground station shown in Fig. 9. In order to flight test small planes, a small autopilot and and data acquisition system is needed. The Kestrel 2.0 autopilot has a mass of 30 gm. It was essential for flight testing the Unicorn UAV. Standard autopilot sensors include a volt meter, differential pressure sensor, absolute pressure sensor, three rate gyros, and three accelerometers. Auxiliary sensors included a current shunt and a GPS antenna. In order to obtain more accurate velocity measurements than those available on the autopilot, a pitot-static tube and a Digikey G-P4V mini 5-inch differential pressure sensor were used. The pitot-static tube had a diameter of 1/8 inch and was purchased from Dwyer Instruments, Inc. Fig. 10 shows the pitotstatic tube and the Digikey differential pressure sensor. The pitot-static tube connected to the Digikey pressure sensor gave an accurate measurement of the difference between the total and static pressure making it possible to measure aircraft velocity with sufficient accuracy.

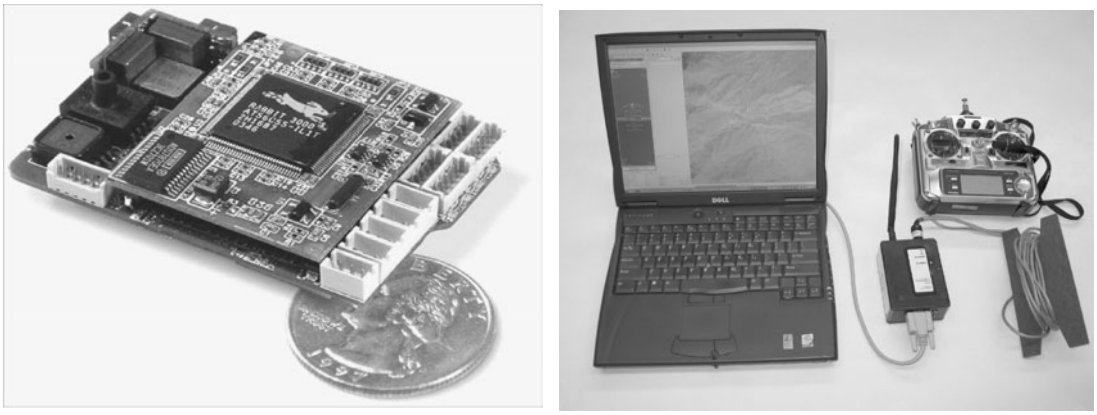

(a) (b)

Figure 9. (a) Kestral 2.0 autopilot, photo used with permission, Procerus Technologies. (b) Ground station.

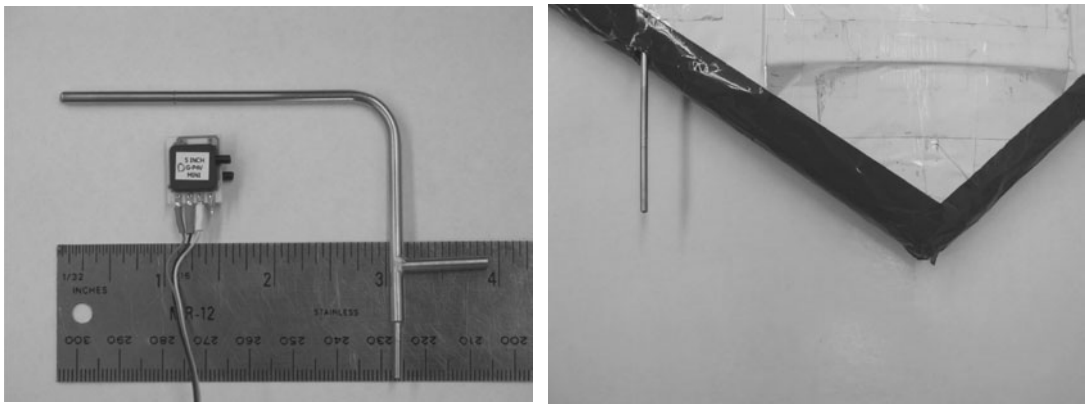

(a) (b)

Figure 10. (a) Dwyer 1/8 inch diameter pitotstatic tube and Digikey G-P4V mini 5 inch differential pressure sensor. (b) Pitotstatic tube shown installed on test aircraft at the leading edge near the nose.

The ground station used for flight testing includes a communications box (commbox) that sends commands to and receives information from the airplane via a 900 MHz shared frequency RF link. The commbox was connected to a laptop computer where a graphical user interface allowed the operator to view measurements made on the airplane inreal time. The user interface was also used to program desired flight settings, plan and upload GPS waypoint flight paths to the UAV, and log telemetry data transmitted from the test aircraft to the ground station.

C. Propeller-Motor Efficiency

The efficiency of the propeller-motor combination measured during wind tunnel testing is displayed in Fig. 11. The data points shown in Fig. 11 are a visual representation of the two dimensional look-up table described in section III.B. The surface shown in Fig. 11 is created by interpolating between the data points. Efficiency values range from 0.22 at high air speeds and low power to 0.53 at mid-range air speeds and high power.

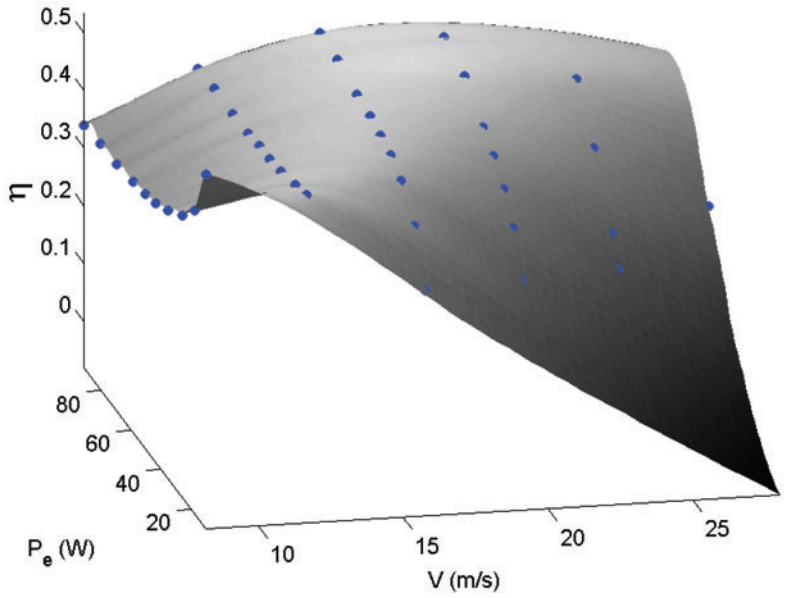

Figure 11. Propeller-motor efficiency surface of a MEGA 16/15/6 brushless motor and a 7 × 4 propeller.

D. Drag Polar

Figure 12 displays the measured drag polar data for the Unicorn UAV. Both forms of the drag polar equation(Eq. (1) and Eq. (2)) can be estimated from this data.

The drag polar data shown in Fig. 12 has errors up to 17% of the total value, even though the data is well behaved. Only a small fraction of the error is due to measurement variation. The majority of the error is a result of instrument error. Table 1 displays the maximum instrument errors that were observed during preliminary testing. It would be valuable for future work to find sensors with reduced instrument error that still meet the limited size and weight requirements of small UAVs.

Table 1. Instrument error for measurements made during wind tunnel testing and flight testing. Values are given at the 95 % confidence level.

Sensor	Instrument Error	Units
voltage	± 0.20	Volt
current	± 0.16	Amp
airspeed	± 0.25	m/s

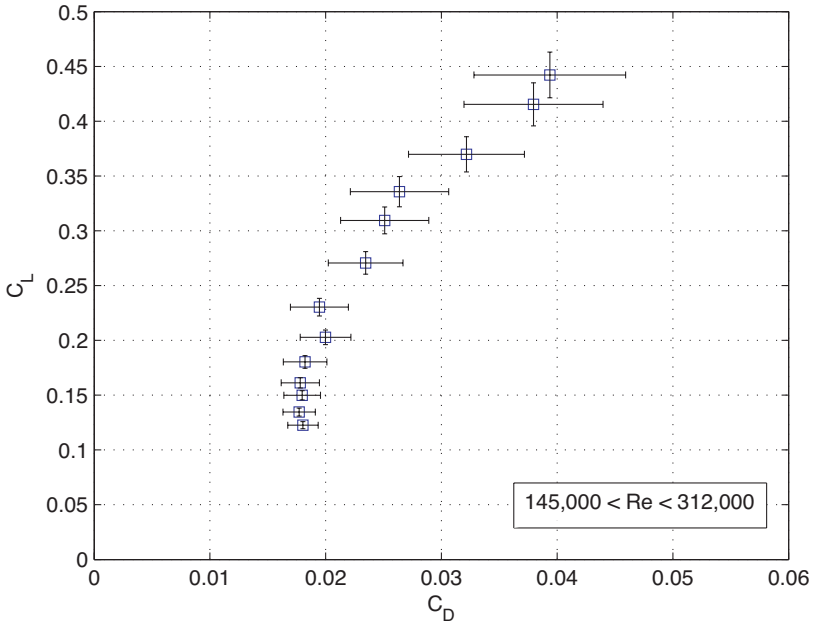

Figure 12. Drag polar of the Unicorn UAV. Error represents a 95 % confidence interval.

To find the coefficients of Eq. (1), the flight test data was curve fit to a second order polynomial. Using this method C_{D_o} was found to be 0.0213 ± 0.0005, K_1 was 0.22 ± 0.02, and K_2 was -0.056 ± 0.004 which gives the following drag polar.

$$C_D = 0.0213 - 0.056C_L + 0.22C_L^2 \tag{29}$$

Eq. (29) is plotted with the flight test data in Fig. 13. The R^2 value for this model is 0.99.

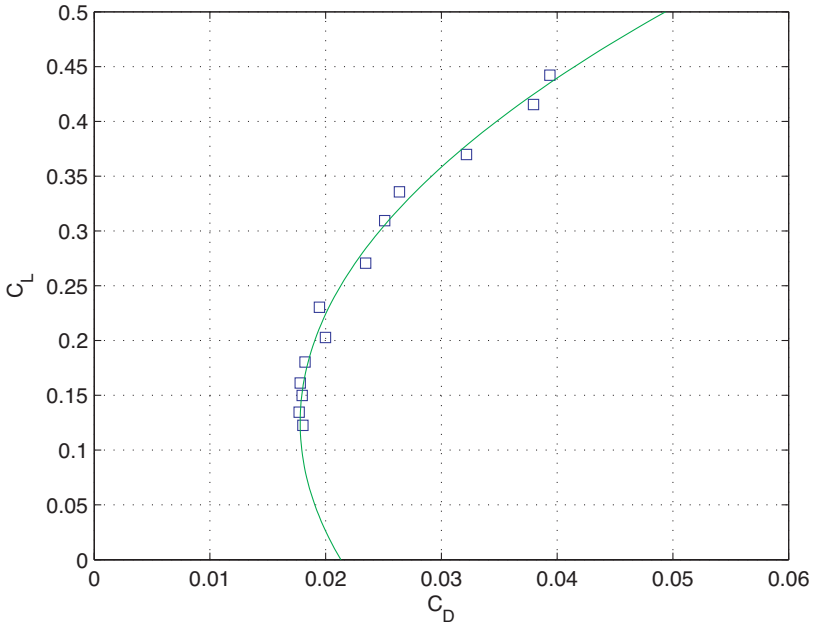

Figure 13. Drag polar superimposed on flight test results.

A plot of C_D vs C_L^2 can be used to find C_{D_o} and K for the drag polar given in Eq. (2). If the data is fit with a straight line, then C_{D_o} is equal to the y-intercept and K is equal to the slope. Fig. 14(a) shows

C_D vs C_L^2 for the Unicorn UAV. C_{D_o} was found to be 0.015±0.001 and K was found to be 0.13±0.03 resulting in

$$C_D = 0.015 + 0.13C_L^2. \tag{30}$$

Figure 14(b) shows the drag polar in Eq. (30) plotted on top of the flight test data. The R^2 value for this model was 0.97.

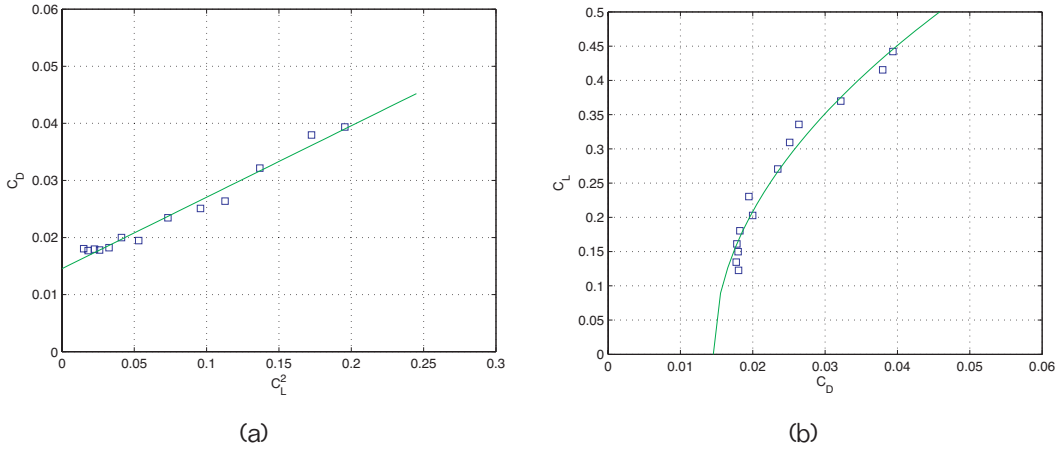

Figure 14. (a) C_D vs C_L^2 for the Unicorn UAV. (b) Simplified drag polar superimposed on flight test results.

The two forms of the drag polar presented here provide slightly different models. The quality of the fit indicates the expanded drag polar of Eq. (29) is a better representation of the drag polar for the Unicorn UAV. This model of the drag polar will be used to find the remaining results presented in this paper.

E. Power Required and Maximum Velocity

Power available and power required are both plotted in Fig. 15 for the Unicorn UAV. Maximum velocity occurred at 22.6 ± 0.3 m/s. When maximum throttle was commanded during flight testing the measured airspeed averaged 22.1 ± 0.25m/s.

F. Minimum Velocity

Minimum velocity was found by programming the autopilot to control a constant airspeed, altitude, and heading, and then reducing the desired airspeed until minimum velocity was reached. As the airspeed approached minimum velocity one of two behaviors was observed. Either the airplane would maintain pitch and heading but could no longer maintain desired altitude and would begin to descend, or the airplane would begin rolling violently to the right and left due to the autopilot's attempt to maintain altitude and heading despite the stall occurring on the wings. When either condition occurred the aircraft's airspeed was recorded as the minimum velocity. For the Unicorn UAV, minimum velocity was found to be 10.5 ± 0.25 m/s. This minimum velocity corresponds to a maximum lift coefficient of 0.44 ± 0.02.

G. Rate of Climb

A plot of rate of climb verses velocity for the Unicorn UAV is shown in Fig. 16(a). Maximum rate of climb was found to be 3.6 m/s and was achieved at an airspeed of 13.4 m/s. Figure 16(b) shows maximum climb angle verses velocity. For the Unicorn UAV the velocity for maximum climb angle is 10.5 m/s. For this aircraft this is also the stall velocity . In order to avoid the danger of stalling a slightly higher airspeed should be used for maximum climb angle.

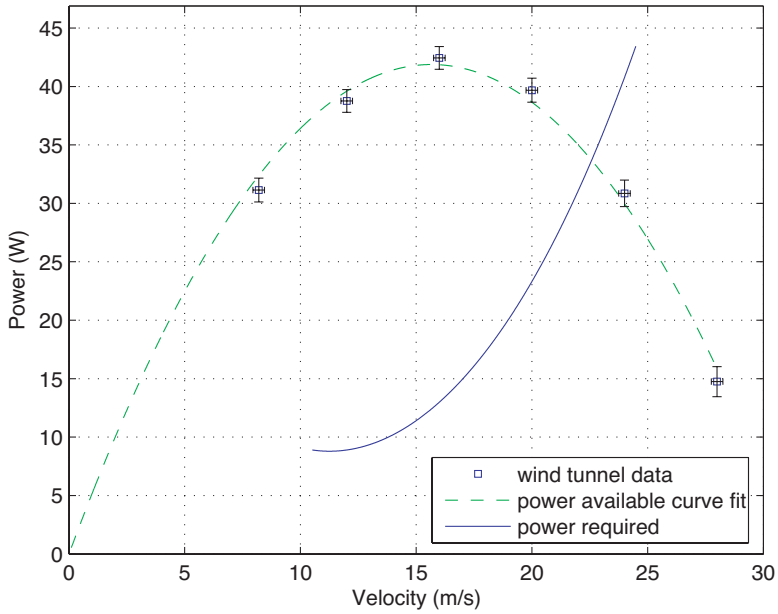

Figure 15. Power available and power required for the Unicorn UAV powered by a MEGA 16/15/6 brushless motor with a 7 × 4 propeller.

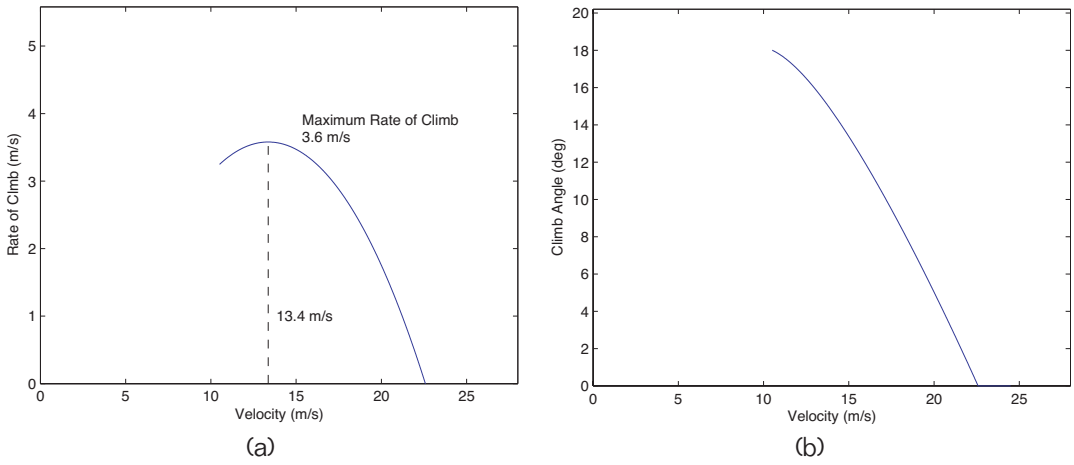

Figure 16. (a) Rate of climb verses velocity. (b) Maximum climb angle verses velocity.

H. Range and Endurance

Graphical results showing velocity for maximum range and endurance appear in Fig. 17. Velocity for maximum endurance is shown on the power required plot (a) and was found to be 11.3 m/s. Velocity for maximum range is shown on the thrust required plot (b) and was found to be 13.2 m/s.

I. Turn Performance

Turn performance parameters found from the drag polar of the Unicorn UAV are shown below in Fig. 18. Minimum turn radius was 13.2 meters, maximum turn rate was 80 deg/s, and maximum bank angle was 69.1 deg. All of these values occur at 18.4 m/s which also corresponds to the velocity for maximum load factor.

J. Model Validation

Flight test results can also be used to validate engineering models. An analytical method for predicting the drag polar of small unmanned aircraft is given by Bowman and Snyder.[13] Predictions made by this method for the Unicorn UAV are presented in Fig. 19. Velocities for the Unicorn UAV range from stall

at 10.5 m/s to maximum velocity at 22.1 m/s. This range corresponds to Reynolds numbers from 145,000 to 312,000. Predicted drag polars for both the low and high Reynolds numbers assuming laminar and turbulent flow are shown in Fig. 19. For the Unicorn UAV it appears that the laminar flow model is more accurate at low Reynolds numbers and that the turbulent model is more accurate at high Reynolds numbers.

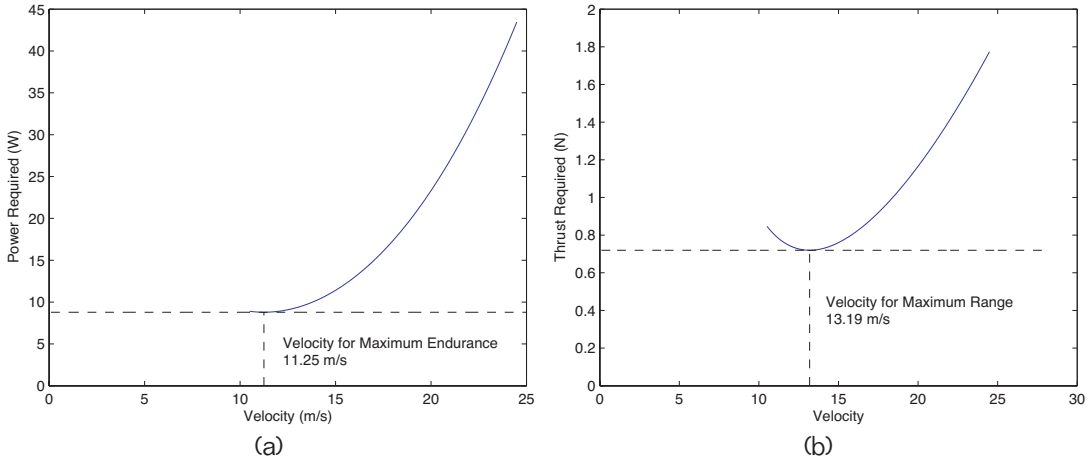

Figure 17. Velocity for maximum range and maximum endurance.

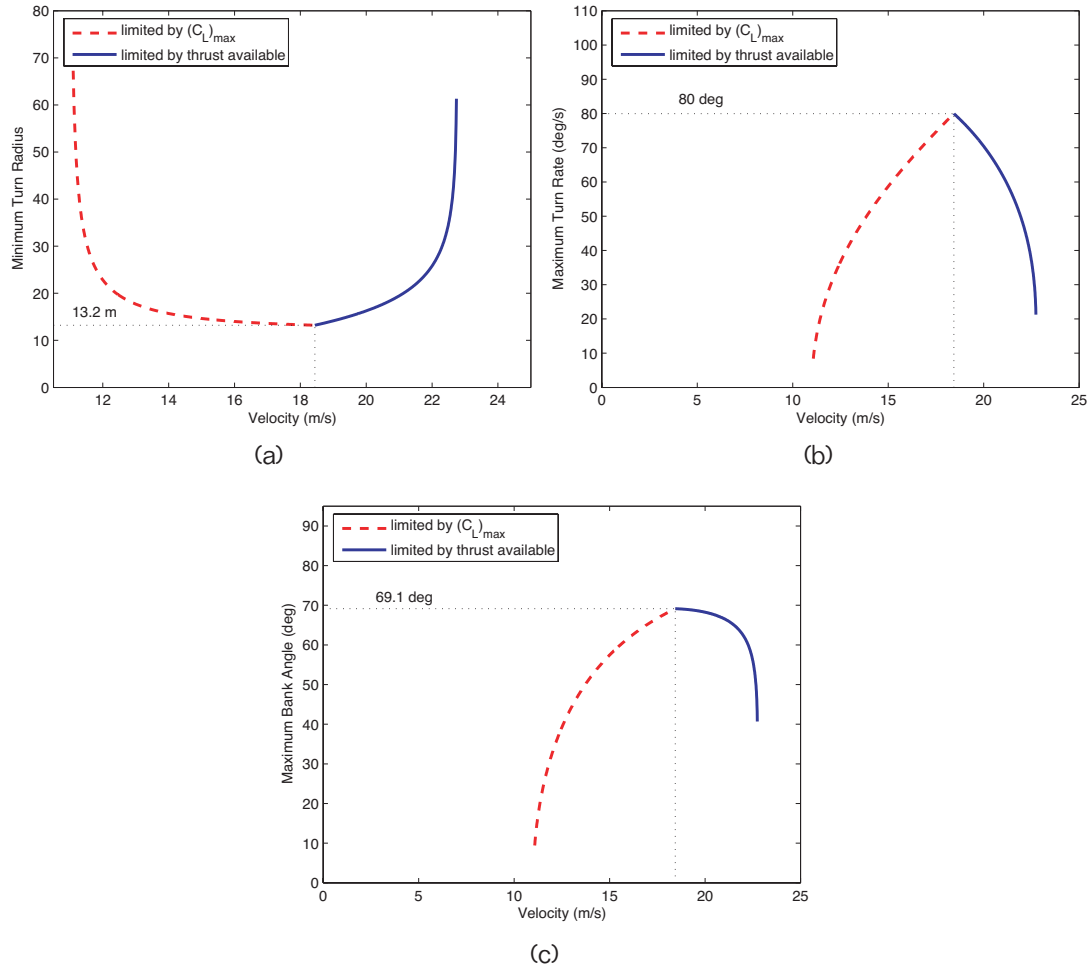

Figure 18. Turn performance parameters for the Unicorn UAV.

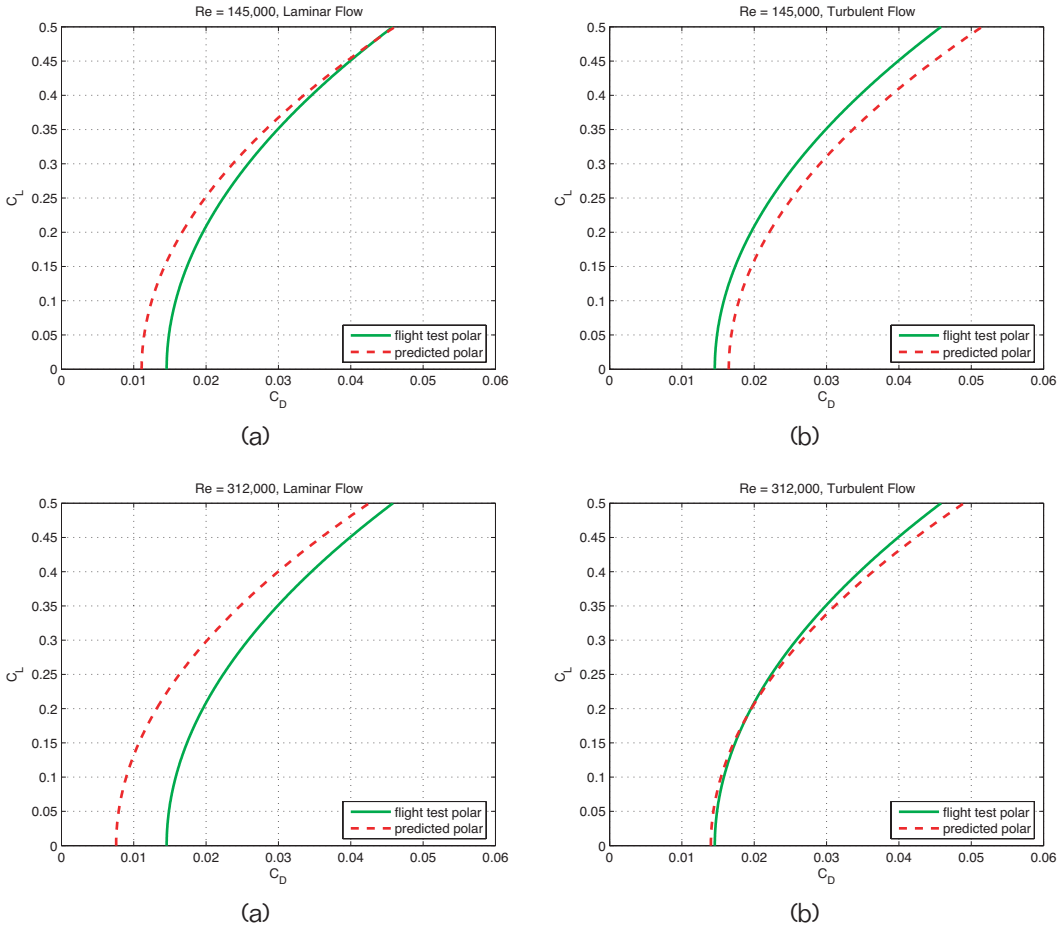

Figure 19. Predicted drag polars verses flight test results.

VI. CONCLUSIONS

Flight test methods have been developed for small electric powered UAVs. These methods have been used successfully to find the drag polar and many performance parameters including range, endurance, climb performance, and turn performance for the Unicorn UAV. Methods consist of measuring aircraft dimensions and properties, wind tunnel testing to characterize the efficiency of the motor-propeller combination, and flight testing to determine the coefficient of lift and the coefficient of drag for the airplane over a range of velocities. The drag polar data found from flight testing was well behaved. However, on a 95 % confidence interval the errors were as large as 17 % of the total value. This error was due primarily to the instrument error in the current and voltage measurement. Using flight test data, $C_D = 0.02 - 0.06C_L + 0.22C_L^2$ was determined to be the drag polar for the Unicorn

REFERENCES

1. Foster, T. and Bowman, J., "Dynamic Stability and Handling Qualities of Small Unmanned-Aerial Vehicles," *43rd AIAA Aerospace Sciences Meeting and Exhibit*, Reno, Nevada, January 2005, AIAA-2006-1023.
2. Higashino, S. and Ly, U., "Development of a UAV Flight-Test Vehicle at the University of Washington," *2nd AIAA "Unmanned Unlimited" Systems, Technologies, and Operations, Workshop and Exhibit*, September 2003, AIAA 2003-6583.
3. Brinker, J. and Wise, K., "Flight Testing of Reconfigurable Control Law on the X-36 Tailless Aircraft," *AIAA Journal of Guidance, Control and Dynamics*, Vol. 24, No. 5, Sep.-Oct. 2001, pp. 903-909.
4. Murray, J. E., Pahle, J. W., Thornton, S. V., S. Vogus, T. F., Mello, J. D., and Norton, B., "Ground and Flight Evaluation of a Small-scale Inflatable-winged Aircraft," *40th AIAA Aerospace*

Sciences Meeting and Exhibit, Reno, Nevada, January 2002, AIAA-2002-0820.

5. Seanor, A., *Flight Testing of a Remotely Piloted Vehicle for Aircraft Parameter Estimation Purposes*, Ph.D. thesis, West Virginia University, Virginia, 2002.
6. Budd, G., "Operation and Research Aspects of Radio Controlled Flight Test Program," *Tech. rep., 1993, NASA Technical Memorandum*, 104266.
7. Williams, W. and Harris, M., "The Challenges of Flight-Testing Unmanned Air Vehicles," *Systems Engineering, Test and Evaluation Conference*, Sydney, Australia, October 2002.
8. Hiller, B., "Estimation of Drag Characteristics of a Fixed Wing Unmanned Aerial Vehicle," *AIAA's 1st Technical Conference and Workshop on Unmanned Aerospace Vehicles*, Portsmouth, Virginia, May 2002, AIAA-2002-3495.
9. Abdulrahim, M., "Flight Performance Characteristics of a Biologically-Inspired Morphing Aircraft," *43rd AIAA Aerospace Sciences Meeting and Exhibit*, Reno, Nevada, January 2005, AIAA-2005-345.
10. Kimberlin, R., *Flight Testing of Fixed-Wing Aircraft*, American Institue of Aeronautics and Astronautics, 2003.
11. Phillips, W. F., *Mechanics of Flight*, John Wiley and Sons, Inc, 2004.
12. Anderson, J. D., *Aircraft Performance and Design*, McGraw-Hill, 1999.
13. Bowman, W. J. and Snyder, D., "A Less Minimalist Approach to Teaching Aircraft Design," *44th AIAA Aerospace Sciences Meeting and Exhibit*, Reno, Nevada, January 2006, AIAA-2006-0094.